PHYSICAL REVIEW A **107**, 032803 (2023)

Influence of single adsorbed atoms on charge exchange during ion-surface collisions

M. A. Romero,[1,2] F. Bonetto,[1,2] and Evelina A. García[1]

[1]*Instituto de Física del Litoral (CONICET-UNL), Güemes 3450, S3000GLN Santa Fe, Argentina*
[2]*Departamento de Física, Facultad de Ingeniería Química, Universidad Nacional del Litoral, Santiago del Estero 2829, S3000AOM Santa Fe, Argentina*

(Received 14 December 2022; accepted 15 February 2023; published 7 March 2023)

Partial and final projectile charge states are theoretically analyzed after Li^+ ions frontally collide with a single-layer graphene surface with potassium atoms adsorbed on it, in the very low deposition limit where the adsorbed atoms negligibly interact with each other. We applied a model based on first principles that accounts for all the details of the surface and is used to describe the resonant charge exchange processes occurring in binary collisions between the projectile and the adsorbate, and between the projectile and the C atoms of the graphene surface located in the surroundings of the adsorption site. Completely different neutral fraction dependences with the outgoing velocity are found for the projectiles scattered by the adsorbate and by carbon atoms located far from the adsorbed atom. In addition, an important influence of the adsorbate is perceived in the neutralization of projectiles colliding with the first and second set of carbon atoms nearest to the adsorption site. For C atoms located at middle-range distances (~6.7 Å), the final charge state of the projectile is not affected by the adsorbate presence, even when an effective interaction between the projectile and the K adsorbed atom is revealed via appreciable projectile level widths.

DOI: 10.1103/PhysRevA.107.032803

I. INTRODUCTION

The charge exchange in dynamic interactions between atoms and surfaces has deservedly attracted a lot of attention in recent decades [1–10]. The problem is intrinsically complex since the charge state of a given projectile colliding with a particular surface depends on many interconnected factors such as the electronic properties of the projectile and the surface, the projectile-surface relative velocity, the collision geometry, the topology of the surface, the presence of impurities or adsorbates, etc. However, it is still unknown how relevant each of these ingredients is. Several studies using both theoretical and experimental approaches have been conducted to shed some light on the matter [6,8,11–26]. On the theoretical side, several approaches have been introduced to attack the problem: (i) models based on a probabilistic description of the resonant charge transfer [27–33]; (ii) an approach based on quantum mechanics formalisms adapting the wave-package propagation (WPP) method to ion-surface interactions [34–38]; and (iii) an *ab initio* time-dependent quantum mechanical formalism where the ion-surface interaction is calculated via the bond-pair model [5,9,39–44]. On the experimental side, and even with limitations, low-energy ion scattering (LEIS) has been demonstrated to be the most effective technique to experimentally determine the final charge state of projectiles after being scattered by a given surface [7,10,17,20,25,33,45,46]. Among the weaknesses of the LEIS technique to study charge transfer processes we can mention the usually large area of the probing beam, the difficulties in separating projectiles scattered by the very first atomic layer and deeper layers [25], and the impossibility to monitor partial charge states of the projectile during the collision process.

Diverse studies have shown that the presence of adsorbates introduces two main modifications in the substrate surface with direct consequences in the dynamic charge exchange between projectiles and surfaces. On one hand, there is a long-range or macroscopic effect linked to a modification in the surface work function caused by the adsorbate presence [47,48]. This effect is largely known for being relevant to numerous applications related to field emission materials, optoelectronics, and plasma physics devices. On the other hand, there is a less studied local effect associated to the modification of the electronic wave functions of the substrate atoms located in the vicinity of the adsorbate. This is precisely the general effect that we attempt to address in the present work: How relevant is the local effect induced by the adsorbate presence to the problem of charge exchange in ion-surface collisions?

The influence of adsorbates in the charge exchange during atom-surface dynamic interactions has been studied in the last three decades and it is still an active topic of current reasearch [34,35,38,44,49–57]. The selection of the impurity adsorbed atom is of key relevance for obtaining significant effects during the charge exchange processes. Alkali atoms such as K or Cs have been shown to introduce large effects in the charge exhange during projectile-surface interactions, mostly due to their low ionization energy or as a result of a particular adsorbate electonic state resonating with the substrate valence band. On the other hand, the selection of the projectile atom is also of importance to probe the sensitivity of charge transfer to the presence of adsorbates on a given substrate. Again, light alkaline atoms such as H or Li have been shown to be very sensitive to the presence of adsorbates when used as projectiles [38,44,56–59]. In particular, the neutralization probability of Li^+ can change from 0% to 100% after being scatttered by a crystalline surface of W(100) with different degrees of Cs deposition [60].

The present work is aimed to theroretically explore how the presence of an impurity of a K atom adsorbed on a single-layer graphene surface alters the charge exchange during the dynamic interaction between this surface and Li^+ projectiles. We also analyze the effect of the adsorbate presence on other physical parameters relevant to the charge transfer such as the broadening and shift of the ionization and affinity projectile energy levels, and the hopping interactions with the carbon atoms in the vicinity of the adsorption site. The analysis allows us to determine a region where the projectile can "feel" the presence of the adsorbate (through modifications in the width or shifts in its energy levels) and, if different, a region where the presence of the adsorbate effectively alters the partial and final charge state of the projectile during the collision process.

A comparison with a previous work, where the charge exhange when H^+ projectiles collide with a graphene surface with K impurities was described, allows us to quantify the influence of the extension of the projectile in the charge exchange process. In addition, via contrasting both results, we can make a conclusion on the relevance of the relative position of the projectile ionization and affinity levels with respect to the valence and conduction bands of the whole surface.

Experimental measurements of the calculated ion fractions with low-energy ion scattering under the conditions assumed in the present work are quite difficult to implement mainly due to two main factors: (i) the complexity in preparing samples consisting of single-layer graphene substrates with such a low deposition of alkaline impurities, and (ii) separating contributions from C atoms in the vicinity of the adsorption site with contributions from other C atoms becomes unfeasible given the usually macroscopic width of the incident beam in the LEIS technique. Alternatively, we can always compare our calculations with the very extreme limit of Li^+ atoms impinging on a clean graphene or highly oriented pyrolytic graphite (HOPG) target surface [39].

II. THEORETICAL APPROACH

A. Description of the atom-surface interaction

The K coverage of the graphene surface is assumed to fulfill the low deposition limit, where the alkaline absorbed atoms are sufficiently distant from each other to assume a null interaction between them. The single-impurity Anderson Hamiltonian [61] is used to appropriately describe both the static interactions between the adsorbate atom and the graphene surface, and the dynamic interactions between the projectile atom and the target surface (either with adsorbed K or with substrate C graphene atoms). The charge exchange is considered to be driven by resonant mechanisms due to the position of ionization and affinity projectile energy Li-2s levels relative to the valence and conduction bands of the surface. Using the projection operator technique [62], the Anderson Hamiltonian can be written as [63]

$$\begin{aligned}\hat{H} = {} & \sum_{\vec{k},\sigma} \varepsilon_{\vec{k}} \hat{n}_{\vec{k}\sigma} + E_0 |0\rangle\langle 0| + E_1 \sum_{\sigma} |\sigma\rangle\langle\sigma| + E_2 |\uparrow\downarrow\rangle\langle\uparrow\downarrow| \\ & + \sum_{\vec{k},\sigma} \left[V^{(1)\sigma}_{\vec{k}a} \hat{c}^{\dagger}_{\vec{k}\sigma} |0\rangle\langle\sigma| + V^{(1)\sigma *}_{\vec{k}a} |\sigma\rangle\langle 0| \hat{c}_{\vec{k}\sigma} \right] \\ & + \sum_{\vec{k},\sigma} (-1)^{p_\sigma} \left[V^{(2)\sigma}_{\vec{k}a} \hat{c}^{\dagger}_{\vec{k}\sigma} |\bar{\sigma}\rangle\langle\uparrow\downarrow| + V^{(2)\sigma *}_{\vec{k}a} |\uparrow\downarrow\rangle\langle\bar{\sigma}| \hat{c}_{\vec{k}\sigma} \right].\end{aligned} \tag{1}$$

For the static adsorption of an alkali impurity (potassium), the expansion of the Hamiltonian [first term, Eq. (1)] is performed over the $\vec{k}$ states, linked to the energy eigenvalues of the clean graphene surface ($\varepsilon_{\vec{k}}$). Its occupation number operator $\hat{n}_{\vec{k}\sigma}$ is given by $\hat{n}_{\vec{k}\sigma} = \hat{c}^{\dagger}_{\vec{k}\sigma} \hat{c}_{\vec{k}\sigma}$. As in [55], we consider for the impurity atom the three charge-state configurations, which correspond to the s-valence level occupied with zero ($|0\rangle$), one ($|\sigma\rangle$), and two ($|\uparrow\downarrow\rangle$) electrons. The total energies E_i ($i = 0,\ 1,\ 2$) of an atom with i electrons are related to the ionization energy of the adsorbed atom ε_I, and to the intrasite electronic Coulomb repulsion U in the s valence orbital, as follows:

$$\begin{aligned} E_1 - E_0 &= \varepsilon_I, \\ E_2 - E_0 &= 2\varepsilon_I + U. \end{aligned} \tag{2}$$

The hopping integrals, $V^{(1)\sigma}_{\vec{k}a}$ and $V^{(2)\sigma}_{\vec{k}a}$, represent the coupling between the $\vec{k}$ states of the graphene surface and the a orbital (K 4s) of the potassium adatom. The superscripts (1) and (2) indicate coupling with the ionization and the affinity levels, respectively. In Eq. (1) the antisymmetry of the two-electron wave function is taken into account through $p_\sigma = 0$ if $\sigma = \uparrow$ and $p_\sigma = 1$ if $\sigma = \downarrow$. In addition, the norm condition of the electronic configuration subspace is considered:

$$|0\rangle\langle 0| + \sum_{\sigma} |\sigma\rangle\langle\sigma| + |\uparrow\downarrow\rangle\langle\uparrow\downarrow| = \hat{1}. \tag{3}$$

The surface-adatom coupling terms, $V^{(1)\sigma}_{\vec{k}a}$ and $V^{(2)\sigma}_{\vec{k}a}$, and the total energies of the selected configurations E_i ($i = 0,\ 1,\ 2$) are calculated via the bond-pair model [64,65].

For describing the dynamic interaction between the Li^+ projectile and the graphene-K adatom surface, the same expression [Eq. (1)] for the Hamiltonian is used. Now, the $\vec{k}$ states in the first term of Eq. (1) include both the atomic orbitals centered on the carbon atoms of the clean graphene, and the K 4s valence states of the adsorbed atom. The core states K 3p are also included since they resonate with the graphene valence band. Analogously, the charge configurations with zero ($|0\rangle$), one ($|\sigma\rangle$), and two ($|\uparrow\downarrow\rangle$) electrons are considered for the 2s valence level of the lithium atom. The variation of the one-electron projectile energy levels, ε_I and $\varepsilon_I + U$, with the projectile-surface distance is calculated from the bond-pair model [64,65] without allowing charge exchange between the atom and the surface. The short-range electron-nucleus and electron-electron interactions are treated within a mean-field approximation. The effect of the long-range interactions, which define the behavior at large normal ion-surface distances, is obtained after considering both the image potential [65] and the energy level shift produced by the dipole potential formed by the adsorbate and its image [34,49,52].

B. Equilibrium process

In order to properly describe the surface formed by the alkaline atom adsorbed on the graphene surface, it is necessary to determine the density matrix of the whole surface. These matrix elements are calculated by using the Green's function formalism, discussed in detail in Refs. [44,56]. Local and partial density of states (LDOS) of the K $4s$ valence states are calculated via the single-impurity Anderson model, after introducing the time-independent Green's functions required, which are obtained via Fourier transform of the time-dependent Green's functions:

$$\begin{aligned} G_\sigma(t,t') &= i\Theta(t'-t)\langle\{|\sigma\rangle\langle 0|_{t'}, |0\rangle\langle\sigma|_t\}\rangle, \\ G^\sigma_{\uparrow\downarrow}(t,t') &= i\Theta(t'-t)\langle\{|\uparrow\downarrow\rangle\langle\sigma|_{t'}, |\sigma\rangle\langle\uparrow\downarrow|_t\}\rangle, \end{aligned} \tag{4}$$

where $\{,\}$ indicate anticommutator. These Green's functions are solved up to second order in the atom-surface coupling term by applying the equation of motion method (EOM) [63]. For the K $3p$ core state, resonant with the valence band of graphene, the LDOS is obtained by considering a noninteracting system (spinless) [66].

The LDOS projected on the surface carbon atoms is obtained analogously to that of K $4s$, with the Green's functions involving the graphene surface states.

The density functional theory (DFT)-based FIREBALL code [67,68] is used to obtain the density matrix elements of the clean graphene surface (required by this model), where the linear combination of atomic orbitals approximation (LCAO) is used to describe the solid surface wave function.

C. Nonequilibrium processes: Finite U-correlated atom states

The time evolution of the Li projectiles charge state during its interaction with the graphene-K adatom surface is calculated via the nonequilibrium Green-Keldysh functions formalism [56]. The neutralization and negative ion formation probabilities at time t, $P^0(t)$ and $P^-(t)$, respectively, read as

$$\begin{aligned} P^0(t) &= \sum_\sigma \hat{n}_{1\sigma}(t) = \sum_\sigma \langle|\sigma\rangle\langle\sigma|\rangle_t, \\ P^-(t) &= \hat{n}_2(t) \equiv \langle|\uparrow\downarrow\rangle\langle\uparrow\downarrow|\rangle_t. \end{aligned} \tag{5}$$

The time evolution of occupations, $\hat{n}_{1\sigma}(t)$ and $\hat{n}_{2\sigma}(t)$, are calculated from the Green-Keldysh functions [69], defined as

$$\begin{aligned} G_\sigma(t,t') &= i\Theta(t'-t)\langle\{|\sigma\rangle\langle 0|_{t'}, |0\rangle\langle\sigma|_t\}\rangle, \\ G^\sigma_{\uparrow\downarrow}(t,t') &= i\Theta(t'-t)\langle\{|\uparrow\downarrow\rangle\langle\sigma|_{t'}, |\sigma\rangle\langle\uparrow\downarrow|_t\}\rangle, \\ F_\sigma(t,t') &= i\langle[|\sigma\rangle\langle 0|_{t'}, |0\rangle\langle\sigma|_t]\rangle, \\ F^\sigma_{\uparrow\downarrow}(t,t') &= i\langle[|\uparrow\downarrow\rangle\langle\sigma|_{t'}, |\sigma\rangle\langle\uparrow\downarrow|_t]\rangle \end{aligned} \tag{6}$$

where $[,]$ and $\{,\}$ indicate commutator and anticommutator, respectively; and $\langle\cdots\rangle$ indicates the expectation value over a wave function that describes the system in the Heisenberg representation. These Green's functions are again calculated by applying the EOM method closed up to second order in the atom-surface hopping terms $V^{(1)\sigma}_{\vec{k}a}$ and $V^{(2)\sigma}_{\vec{k}a}$, as detailed in Ref. [56].

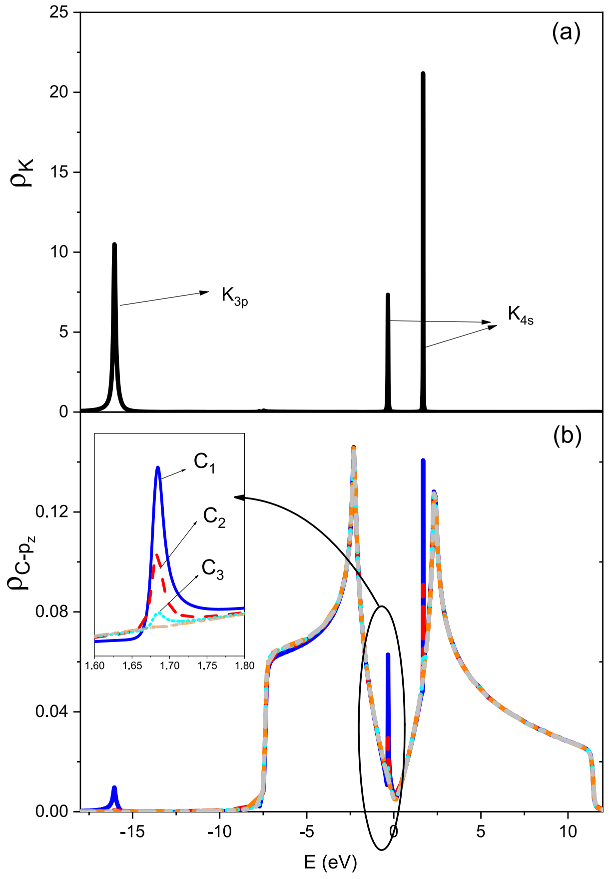

FIG. 1. (a) Local density of states projected on the K atom where the contributions of the K $3p$ and K $4s$ states are indicated. Inset: Top view of the position of the adsorbed K atom on the graphene layer. The carbon atoms labeled C_n ($n = 1,\ldots,8$) correspond to one of the nth nearest carbon atoms to the adsorption site. (b) Graphene plus K partial p_z density of states projected on C atoms at different distances from the K adatom; the color line corresponds with that of the C atoms plotted in the inset of (a). Solid blue, dashed red, short dot cyan, dashed dot orange, and dashed dot-dot gray lines correspond to C_1, C_2, C_3, C_4, and C_5 atoms, respectively. Inset: the region circled in (b) is zoomed in in order to show the influence of the K adatom on the projected DOS on carbon atoms located at different C-K distances.

III. RESULTS AND DISCUSSION

A. Density matrix of graphene plus adatom

The most stable adsorption site for alkali atoms on graphene is located right above the center of the graphene hexagon (hollow site). The adsorption distance between the K adsorbed and the graphene layer is around 4.9 a.u. (a.u., atomic units are used) [70–72].

In our previous works [55,56] we extensively studied the details of the adsorption process: the description of the charge transfer between the adatom and the surface, and the complete density matrix system (graphene + impurity). In the present study, we focus on the diagonal elements of the graphene plus potassium density matrix (local and partial density of states). In Fig. 1 we show the DOS of the full surface projected on the adsorbed K atom, $\rho_K(E)$, and on the different C atoms of the graphene surface, $\rho_C(E)$. In this plot, the zero energy corresponds to the Fermi level of a clean graphene surface.

The LDOS projected on the K atom [Fig. 1(a)] presents typical features of weakly coupled systems [63], due to quantum interference effects introduced by all the C atoms with non-negligible interaction with the K adsorbed atom [55]. As expected, the p_z LDOS projected on the different neighboring C atoms [Fig. 1(b)] reveals that the modifications introduced by the K adsorbed atom become less important when the C-K lateral distance is increased. An almost null influence is observed for C_4 and beyond carbon atoms [see inset of Fig. 1(b)]. Therefore, from the absorption point of view, the presence of the K atom only introduces local modifications in the density of states of graphene, laterally extending up to around 10 a.u. (up to fourth nearest neighbors).

B. Hamiltonian parameters for the scattering process

The energy levels and hopping parameters are calculated via the bond-pair model developed in Refs. [64,65]. A suitable calculation of these parameters requires a proper set of atomic bases for calculating the one- and two-electron atomic integrals, and an appropriate description of the surface electronic structure based on a linear combination of atomic orbitals (LCAO) expansion of the band states. The one-electron hopping term $V_{\vec{k}a}^{(1,2)\sigma}$ includes one- and two-electron contributions determined by performing a mean-field approximation together with an overlap expansion of the many-body Hamiltonian. We use the Huzinaga [73] atomic basis for Li, C, and K atoms with the largest Gaussian basis sets.

For the resonant charge exchange during the collision between Li^+ ions with the graphene plus K surface, we consider different scatter sites: the K atom and six nonequivalent carbon atoms located closer to the impurity with different lateral distances. In Fig. 2, we show top and transverse views of the projectile-surface interaction. The C atoms labeled C_n, with $n = 1, 2, \ldots, 6$, correspond to the first, second, third, and, in general, the nth nearest neighbors to the adsorption site. A carbon atom labeled with C indicates that it is sufficiently far away from the K adatom to consider a negligible K-C interaction (the scattering with this atom should be equivalent to that of a pristine graphene).

For the calculation of the charge exchange during the collision we differentiate two scattering situations: the interaction between the Li^+ projectile and the K adatom, considering the interaction with its six carbon atom nearest neighbors; and the interaction between the Li^+ projectile and a C_n ($n = 1, 2, 3, 4, 5, 6$) carbon atom including in this case the interaction with its three carbon atom neighbors plus the K adatom. When the scattering site corresponds to a C atom far away from the adsorption site, the interaction with the impurity is not present. The collision is frontal, i.e., the incoming and outgoing ion trajectories are assumed perpendicular to the graphene surface, with a constant velocity. The kinetic energy loss of the projectile in the binary elastic collision with the target atom is taken into account in our calculation. Thus, $E_{\mathrm{out}} = \lambda E_{\mathrm{in}}$, where E_{out} and E_{in} are the exit and incoming projectile energies, respectively, and λ is the kinetic energy loss factor [45]. For the head-on collision geometry considered (scattering angle of 180°), λ is equal to 0.484 for Li-K, and it is equal to 0.069 for Li-C collisions.

The dependence of the Li 2s energy levels with the ion-surface distance are shown in Fig. 3(a) for the different scattering centers. The ionization $\varepsilon_I = E_1 - E_0$ and affinity $\varepsilon_A = \varepsilon_I + U$ levels are calculated as in Ref. [44]. Irrespective of the scattering center, the zero distance corresponds to the scatter site position, even when the K adsorbed atom is 4.9 a.u. above the graphene surface layer. At short distances, the pronounced downshift observed is due to a dominant attractive electron-nucleus interaction, while the behavior at large distances is determined by both the graphene image potential [74] and the energy level shift caused by the adsorbate and its image dipole potential [34,44,49,52]. It is relevant to note in this figure that, as expected, the energies of Li tend to those of clean graphene when the C_n-K lateral distance increases. Convergence is reached for a C_4 (fourth nearest neighbors) carbon atom. This fact does not imply that the charge transfer during the dispersion by C_4 and C (clean graphene) will be exactly the same. The couplings with the adsorbate might still be present and, in that case, they will be revealed by the energy levels' hybridization widths [56]. In Fig. 3(b) we plot the Li ionization hybridization widths, $\Gamma(\varepsilon_{\mathrm{ioniz}})$, when the Li projectile is scattered by the K adatom and the different carbon atoms, C_n, as a function of the projectile-scatter atom distance. In the inset of Fig. 3(b) we can observe that even when there are no differences in the energy levels of a C_6 (sixth nearest neighbor) and a carbon atom, C, located far away from the adsorbate, there are still some differences exposed by the hybridization widths. This remark indicates that (i) the local effects extend beyond the fourth nearest neighbors (C_4) as suggested by the energy levels analysis, and (ii) the hybridization widths are more sensitive to the K adatom presence than the energy levels. Convergence for the hybridization widths (not shown) is reached for C_8 (eighth nearest neighbors), which corresponds to a lateral distance of 14.5 a.u. from the adsorbate.

C. Ion charge fractions after collision process

In Fig. 4 we present the calculated final ion fraction dependence on the exit velocity, after Li^+ projectiles frontally collide with both a K adatom and the C_n carbon atoms of the graphene layer located at different distances from the potassium atom adsorbed on it.

In general terms, when Li^+ projectiles are scattered by K, C_1, and C_2 atoms, smooth oscillations in the charge fractions as a function of the exit velocity of the ion (v_{out}) can be observed. These oscillations are typical of target surfaces with localized valence states [23,56,75], such as the K 4s valence state introduced by the adsorbate in the present situation. The oscillations practically disappear when the distance between the adatom and the scattering centers goes beyond the third nearest neighbors. The ion fractions obtained after Li^+ projectiles collide with C_4 and C_6 atoms show a similar dependence with the exit projectile velocity as that of carbon atoms, C, of a clean graphene surface. Convergence for the ion fraction magnitudes is reached for sixth nearest neighbors, C_6, even when differences in the hybridization widths [see inset of Fig. 4(b)] indicate a not null C_6-K interaction. Very few

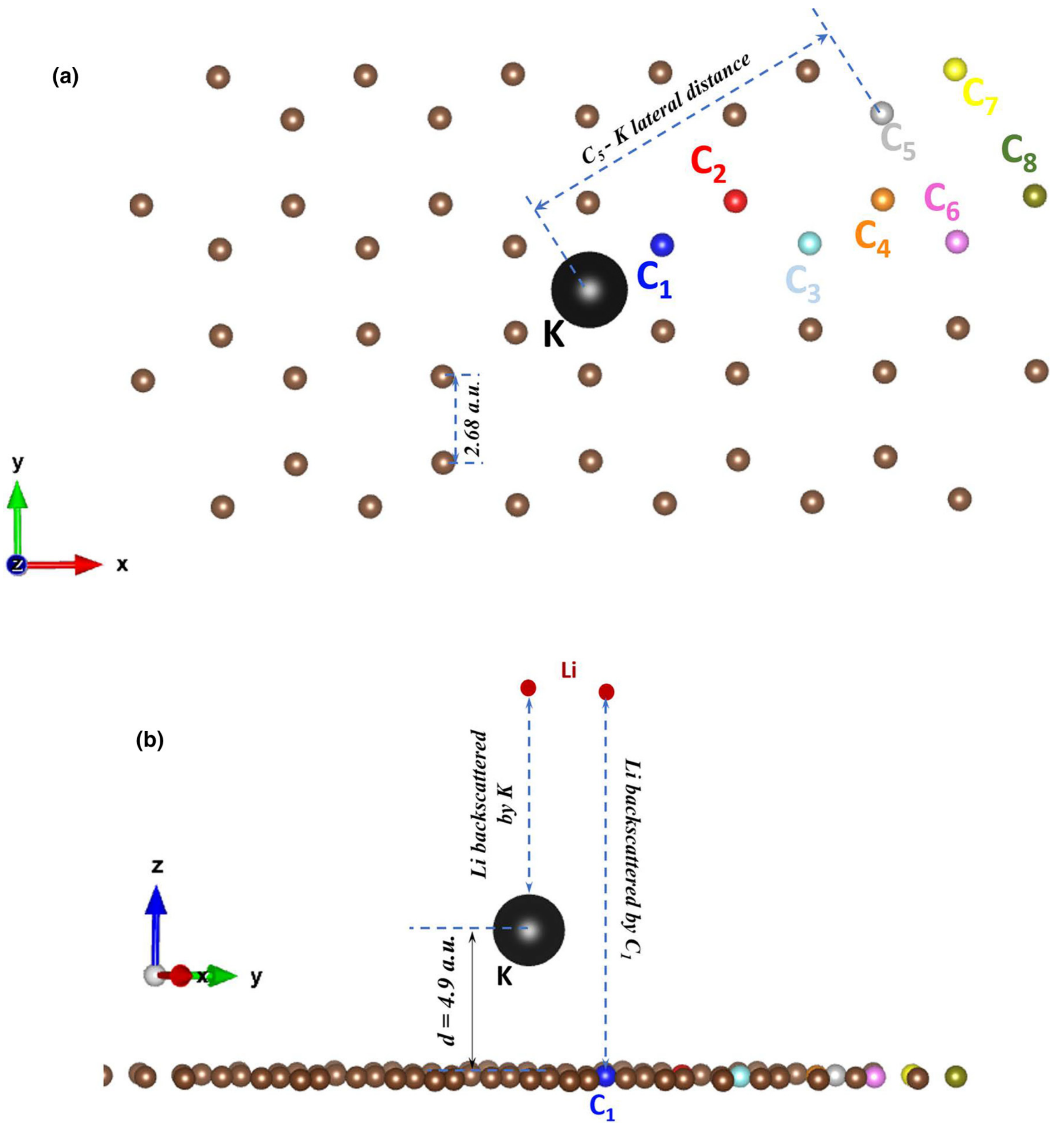

FIG. 2. Top (a) and lateral (b) views of the collisional system studied. In (a) the lateral distance of the different carbon atoms with the adsorbed K atom is indicated. In (b), the scattering of the Li projectile with both the K adatom and one of its nearest carbon atoms, C_1, is sketched. The K-graphene adsorption distance is also shown.

experimental measurements of the charge exchange between Li^+ projectiles and a graphene surface have been reported so far in frontal scattering geometry. However, the magnitudes of the neutral fractions obtained for a pristine graphene surface (∼20%) are comparable to that reported in the forward scattering configuration [39]. It is worth noting also that, for most of the exit energies studied, the negative ion fractions increase for C_n atoms closer to the impurity´s adsorption site.

Going into more detail and interrelating results shown in Fig. 4 with information provided by Fig. 3, we can observe that the energy levels for K and C_1 "map" the same density of states regions [see in Fig. 3(a)], although with a distance shift as a consequence of the K-graphene adsorption distance. In addition, from Fig. 3(b) we can see that their hybridization widths are qualitatively similar, taking into account, again, the distance shift. These remarks means that, for the same incoming and exit velocity, the final charge state of the projectile should be similar in both cases. However, having the same incoming and exit velocities is not possible due to the quite different binary kinetic loss factors for Li-C (0.07) and for Li-K binary collisions (0.4879), implying that Li projectiles with a fixed incoming energy will be scattered by K atoms with an energy 7 times higher than those scattered by C atoms. Then, for having the same exit velocity (as plotted in the previous figures), projectiles scattered by C will have a much larger incoming velocity than those impinging with K. As a consequence, the Li-C interaction time at the incoming path will be much lower than that of the Li-K, resulting in lower neutral and negative ion fractions at the end of the Li-C incoming path. All these aspects of the charge exchange

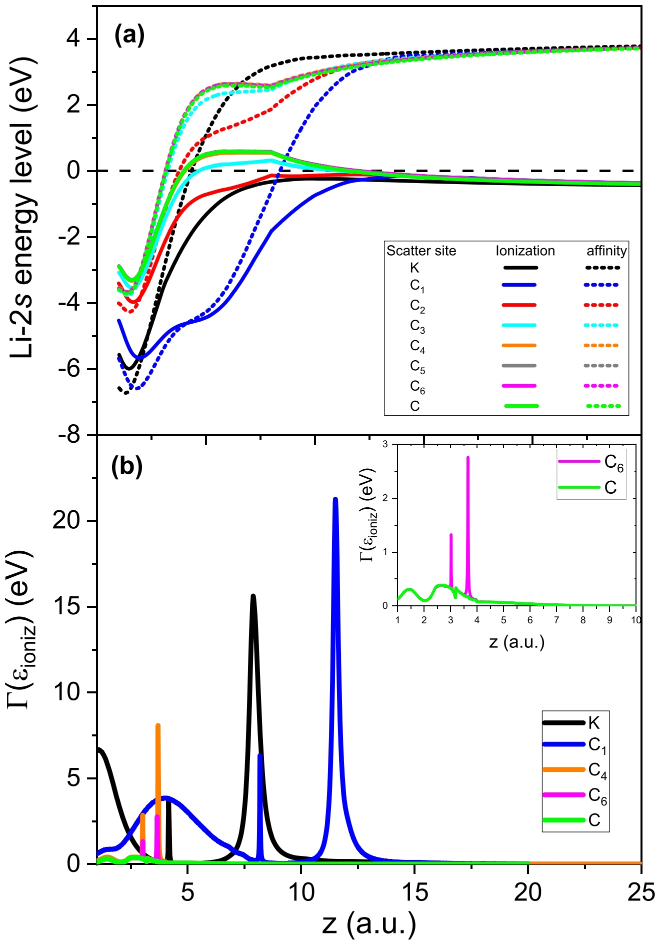

FIG. 3. (a) Ionization and affinity 2*s* energy levels for the Li projectile colliding with the K adatom and carbon atoms of the graphene layer located at different distances from the adsorbate. The corresponding hybridization widths of the ionization Li 2*s* level are shown in (b). Both are plotted as a function of the projectile-scatter atom distance. The differences between hybridization widths of a sixth nearest neighbor, C_6, and a carbon atom located far away from the adsorbate, C, are emphasized in the inset of (b).

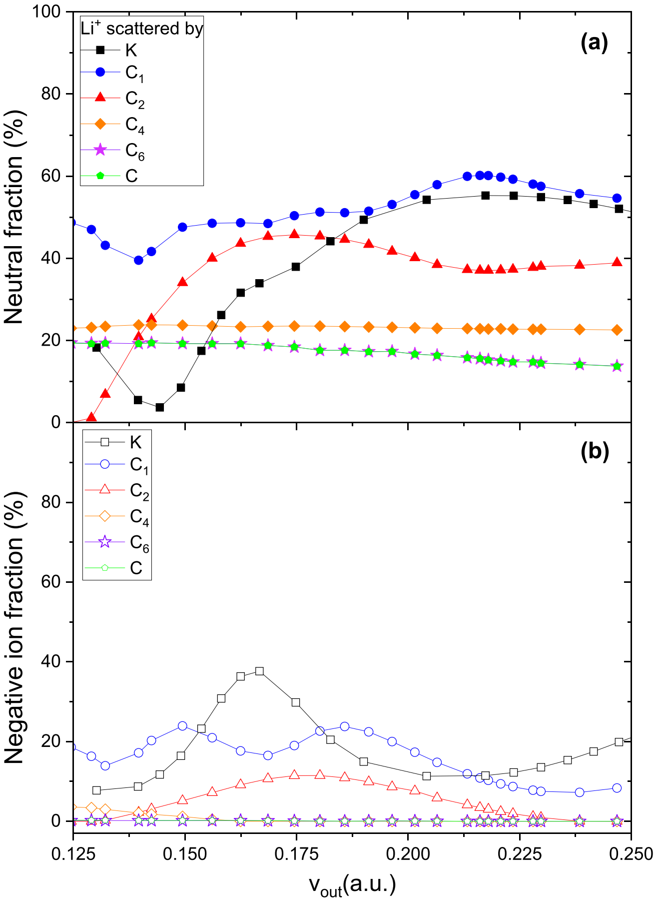

FIG. 4. Neutral (a) and negative (b) ion fractions calculated for Li^+ frontally colliding with the K adatom and the different carbon atoms of the graphene layer located in the surroundings of the adsorption site.

process are explored in Fig. 5 where the Li 2*s* energy levels and their widths, jointly with the surface density of states, are plotted as a function of the projectile-scatter atom distance for collisions with K and C_1 atoms (left panel). The corresponding partial and final neutral fractions as a function of the projectile position are plotted for incoming and outgoing trajectories (right panel, Fig. 5). In this figure is also shown the direct link between the ionization and affinity energy levels and their widths at a given distance with the corresponding change in the neutral and negative projectile charge state, respectively. Here, we can observe that the peak structure (indicated through circles in the figure) of the energy levels widths that are shifted when changing from K to C_1 scattering centers directly correspond to shifted characteristics in the neutral and negative ion fractions.

In the region closer to the surface ($z < 3\,\mathrm{a.u.}$), the hybridization level widths for the Li-K collision mainly correspond to the interaction with the neighboring carbon atoms [see inset in Fig. 5(a)], since the ionization and affinity level do not resonate with the K DOS. In contrast, hybridization widths corresponding to Li-C_1 collisions are more extended [up to $z \sim 6\,\mathrm{a.u.}$; see Fig. 5(b)], leading to a faster increasing neutral ion fraction in the beginning of the incoming trajectory [see Fig. 5(c)]. However, and mainly due to the velocity effects (less interaction time linked to a higher incoming velocity), the projectile neutral fraction for Li-C_1 collisions remains lower than that of Li-K at the end of the incoming trajectory [see Fig. 5(c)]. At the exit trajectory, where the outgoing velocity is the same in both cases, the more extended nature of the interaction widths for the Li-C_1 makes the neutral fraction grow faster than that of the Li-K collision. As a result of these counteracting effects, the final neutral fraction is almost the same for Li-K and Li-C_1 collisions [Fig. 5(c)] for the exit velocity analyzed ($v_{\mathrm{out}} = 0.23\,\mathrm{a.u.}$). Finally, the drop in the neutral fraction observed in both cases for large distances (shifted about 5 a.u. from each other) is a direct consequence of the peak in the energy width [circled in orange in Figs. 5(a) and 5(b)] that allows electronic loss to the conduction band.

Negative ions are practically not generated in the incoming trajectory of Li^+ ions colliding with C_1 carbon atoms [see Fig. 5(d)]. Three main factors contribute to this behavior: (i) the large incoming velocity (when compared to the

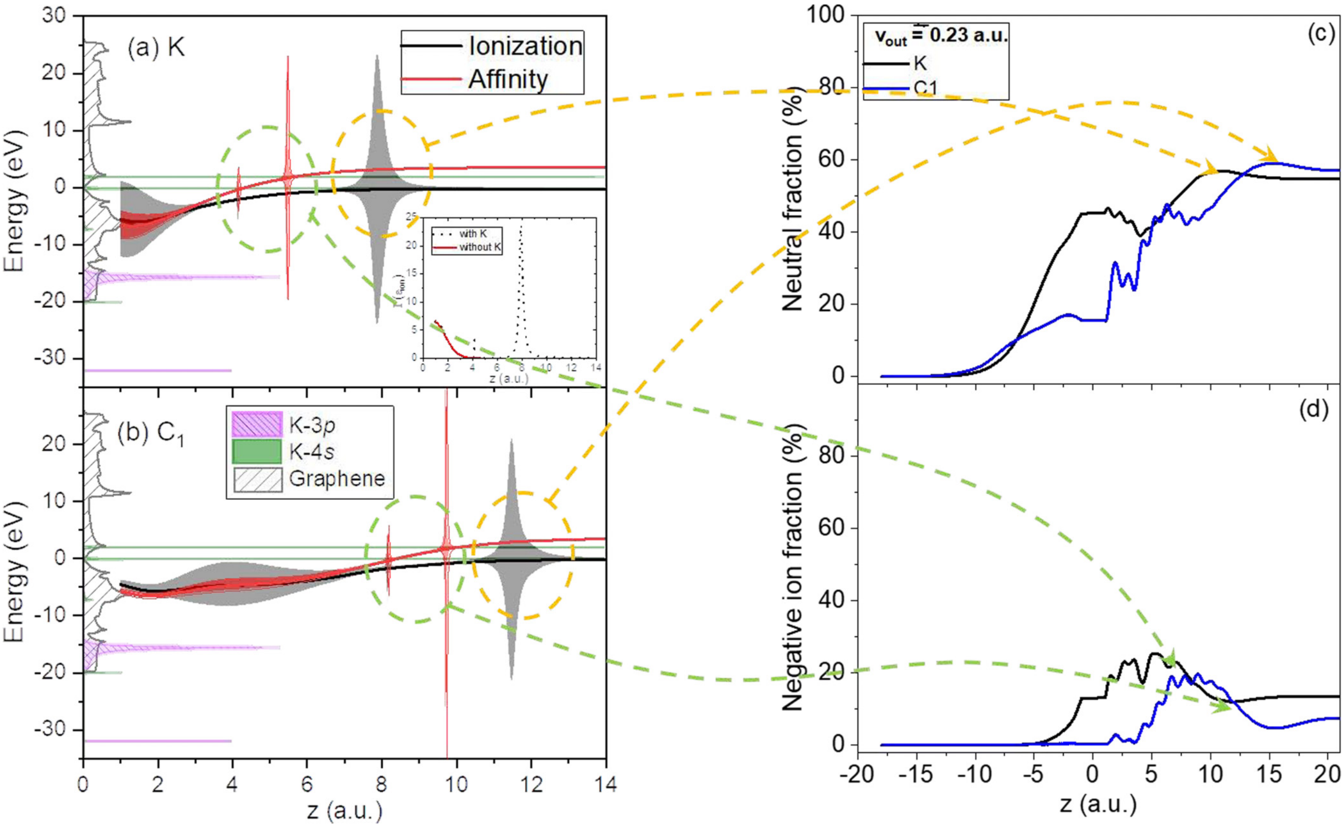

FIG. 5. Left panel: The energy levels and their corresponding widths (shown as error bar) as a function of the projectile-scatter atom distance for Li projectiles colliding with K (a) and C_1 (b). On the vertical axis the local DOS of the surface is shown as shadowed areas, allowing one to identify the region of the DOS mapped by the energy levels. The inset in (a) shows the ionization hybridization width when the K adatom is present (dotted black line) and absent (solid cyan line) in the collision. Right panel: Corresponding neutral (c) and negative ion (d) fraction evolution during the trajectory of the projectile. Negative and positive values of z correspond to the incoming and exit trajectories, respectively. Black (mostly upper) line corresponds to collisions with the K adatom and blue (lower) line corresponds to collisions with C_1 atom. The green dashed arrows indicate the direct connection between the different features of the energy levels with relevant changes in the neutral and negative ion fractions.

Li-K case), (ii) the low formation of neutrals in the incoming trajectory, and (iii) the low interaction width of the affinity level that enables the capture of a second electron. In contrast, Li projectiles that collide with K exhibit a relevant formation of negative ions in the incoming trajectory mainly due to the large interaction level width in the spatial region closer to the surface. In the outgoing trajectory, the increasing neutral fraction in Li-C_1 collisions makes the capture of a second electron more probable up to distances around 8 a.u. where the energy level crosses the Fermi level and the electron loss processes are favored with a consequent drop in the negative ion fraction (indicated with dark green circles and arrows). The same features in the energy level and its width are observed in Li projectiles colliding with K. However, the affinity level crosses the surface Fermi level at about 4 a.u., causing a similar drop in the negative ion fraction in Li-K collisions, but shifted about 4 a.u. to spatial regions closer to the surface. As a result, the final negative ion fraction is comparable in both cases with values on the order of 10% (for the analyzed exit velocity).

The charge exchange in collisions between Li^+ projectiles with carbon atoms located farther from the adsorption site is quite different, as revealed by the neutral and negative ion fraction dependences with the exit velocity (Fig. 4). In Fig. 6(a) we show the Li 2*s* ionization and affinity energy levels with their widths as a function of the distance to the graphene surface z for collisions between Li projectiles and C_6 carbon atoms (sixth nearest neighbors of the adsorption site). The peak structure in the hybridization widths can be directly associated to the interaction with the impurity [see the LDOS on the left side of Fig. 6(a) and the inset in Fig. 3(b)]. The remaining regions of the hybridization width correspond to the interaction with the carbon atoms considered in the collision. For high velocities (short interaction times), the subtle differences between a C_6 atom and a carbon atom C, located far away from the K adatom, are expected to be averaged away and the final charge state of the projectile should be the same in both cases [as observed in Figs. 4(a) and 4(b)]. On the contrary, for low velocities or higher interaction times, the projectile can "see" the slight differences in the hybridization widths of C_6 and clean C, enhancing in this way the contrast in final charge fractions for both collisions. We explore this concept in Fig. 6(b) where the calculation of neutral and negative ion fractions for C_6 and C is extended to lower exit velocities. In this figure we can observe that for velocities lower than 0.10 a.u., small but still visible differences in neutral fractions

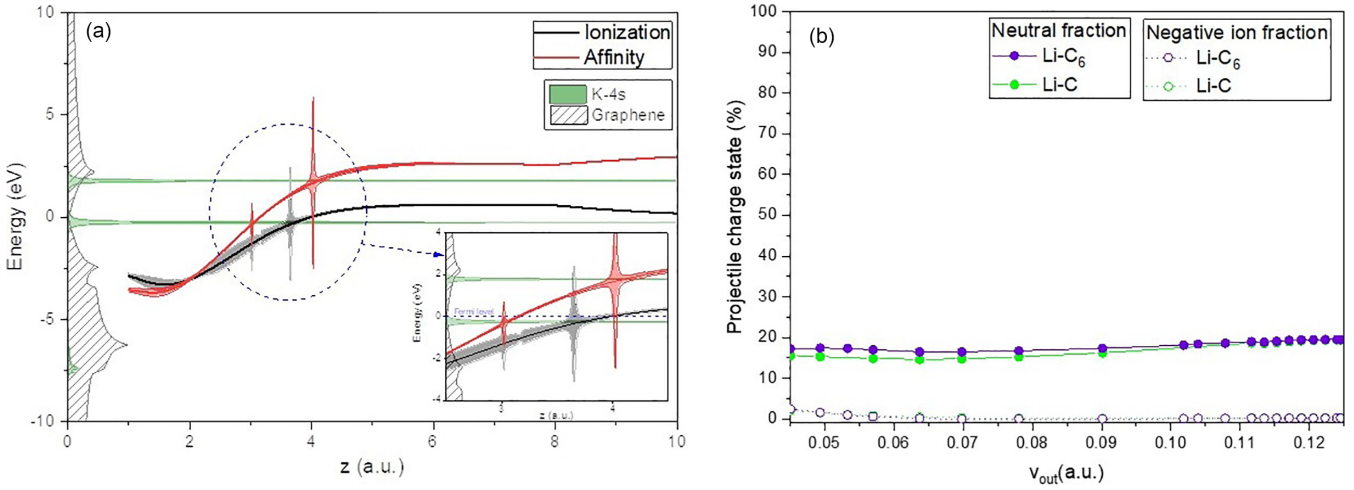

FIG. 6. (a): Ionization and affinity Li 2*s* energy levels and their widths (shown as error bars) as a function of the distance of the graphene surface for collisions between Li^+ projectiles and C_6 atoms. The local DOS projected on the scatter site is also shown (shadowed areas). Inset: The region where changes are introduced by the presence of the adsorbate is zoomed in to highlight that the added peaks in the ionization energy level are centered below the Fermi energy, favoring electronic capture. (b) Neutral and negative final ion fractions for Li-C_6 and Li-C collisions. The light differences in the energy level widths lead to subtle differences in the neutral fractions for the low-energy regime.

can be appreciated (the *y* scale is as in Fig. 3, to directly compare them). The differences between C_6 and C in the energy level widths are basically two peaks appearing in the C_6 energy level widths between 3 and 4 a.u. where the energy level lies below the Fermi level [see inset of Fig. 6(a)]. Therefore, and if the projectile is able to detect these differences, the electronic capture for Li-C_6 collisions would be favored over Li-C collisions, leading to a higher neutral fraction for Li projectiles colliding with C_6 [see Fig. 6(b)].

D. Projectile relevance in the charge exchange process. Comparison with H^+-graphene plus K system

In previous works we studied the head-on collision of H^+ with an alkali covered graphene surface [44,56,57]. Hydrogen is a suitable projectile choice for studying charge exchange since the ionization and affinity energy levels overlap with the bands of the alkali plus graphene surface, favoring in this way the ion-surface resonant charge transfer process. After hydrogen, lithium is the second lightest alkaline element, which makes it an appropriate choice to probe the presence of adsorbate or impurities in surfaces through dynamic charge transfer. From the experimental point of view, lighter elements used as projectiles allow studying a wide variety of surface via low-energy ion scattering spectrometry [76]. The collision between Li^+ and alkali and halogen covered metal surfaces has been extensively studied [13,49,52,57,77,78], but not with an alkali covered graphene.

In Fig. 7 we compare the present results using Li^+ projectiles with previously reported data where H^+ was used as a projectile in dynamic interactions with the same surface and under identical collisional conditions (frontal collisions and similar range of exit velocities). In this way, we are able to discriminate the pure effects of the projectile on the charge exchange. In this figure we show the neutral and negative charge fractions for both projectiles binary colliding with the adsorbed K atom, and with a C atom on the clean graphene surface. To directly compare these results, the range of exit velocities chosen corresponds to that used in the present work.

For projectile ions colliding with the impurity (left panel), we can observe that the general trend and the ion fraction magnitudes are similar to both H^+ and Li^+, suggesting that the common features to both collisions are of crucial importance. In a more detailed analysis, at high exit velocities, the neutral fractions have similar values, while H neutrals are more likely to be scattered for lower exit velocities. In the Li^+-K case, the neutrals are mainly formed due to the interaction of the K adatom with the first neighboring carbon atoms with the impurity; however, for H^+-K collisions the final neutral fraction obtained is mainly due to the interaction of H^+ with the K 3*p* state broadened by the interaction with the valence band of graphene [56]. At low velocities, the larger neutral fraction obtained for H^+ when compared to that of Li^+ is a consequence of an H^+ ionization level lying well below the Fermi level of the surface, resonating with the 3*p* state of the adsorbate. In contrast, the lithium ionization level lies below but quite close to the surface Fermi level, making the electron loss processes more likely due to the non-negligible interaction hybridization widths at large distances. For negative ion fractions [Fig. 7(b)], both affinity levels lie well above the Fermi level in the conduction band leading to similar magnitudes of negative ion fractions. However, more oscillations are observed for H^+-K collisions mainly due to a deeper H affinity level interacting with several localized K states. In addition, the H affinity level crossing the deep K 4*s* localized state introduces more important correlation effects that contribute to the oscillations observed.

When comparing how sensitive both projectiles are to the presence of the K adsorbate in collisions with neighboring carbon atoms, the interaction between the projectile and the C atoms (as revealed by the hybridization energy level widths) extends up to the fifth and eighth C atoms' nearest neighbors of the impurity, for H^+ and Li^+ projectiles, respectively.

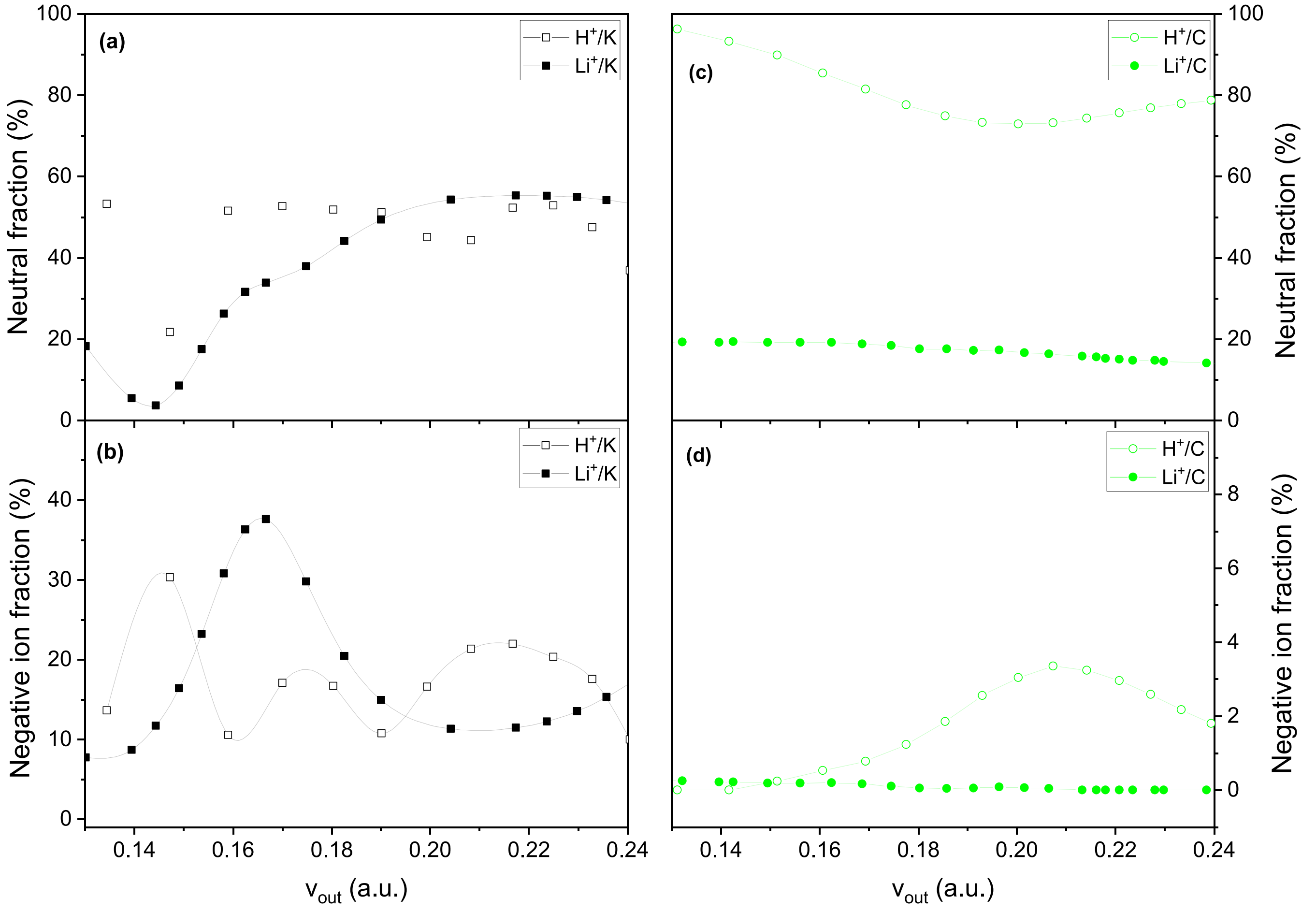

FIG. 7. Neutral (a), (c) and negative (b), (d) ion fractions as a function of exit velocity of the projectile when Li^+ and H^+ are scattered by the impurity K (left panel, black symbols), and by a C atom of a clean graphene surface (right panel, green symbols).

The more extended character of the electronic wave function of Li relative to H atoms allows the projectile to sense the presence of the K adatom at larger distances. Alternatively, the final charge state of the Li projectiles can evidence the presence of the impurity only in collisions with up to C_6 atoms (sixth nearest neighbors from the adsorbed atom), even when the interaction with the K adatoms is not negligible at these distances (12.7 a.u.). Similar findings were recently reported by Bahrim [38] in other collisional systems, using the WPP method.

Strong differences are observed in the neutral fractions for H^+ and Li^+ projectiles colliding with a clean C atom [see Fig. 7(c)]. Much higher neutral fractions are obtained for H^+-C collisions mainly due to an ionization energy level positioned well below the Fermi level and resonating with the graphene valence band during the whole projectile trajectory [56]. In contrast, the Li ionization energy level for Li^+-C collisions remains above the graphene Fermi level for projectile-surface distances relevant to the charge transfer [see Fig. 6(a)], allowing for electronic loss and consequently less formation of neutral particles. The negative ion formation [see Fig. 7(d)] is practically null for both projectiles colliding with a clean C for the explored range of exit velocities. The affinity levels of both projectiles positioned well above the Fermi level conduct to a very low formation of negative ions, which reaches to about 4% for H^+-C collisions. This difference can be attributed to an H^+ affinity level closer to the Fermi level and higher interaction widths than those of the Li^+-C system. Unlike the oscillatory trends observed for charge fractions in H^+-K and Li^+ collisions, charge fractions obtained for collisions with a clean graphene C atom show a smooth dependence on the exit projectile velocity, mainly due to the extended (nonlocalized) features of the graphene DOS.

Finally, it is relevant to mention that our calculations of the neutral and negative ion fractions after H^+ and Li^+ collide with clean graphene C atoms are consistent with measurements previously reported in similar systems such as H^+-HOPG [6,8,26,43], H^+-C_{60} [6,8,24,26,43], or Li^+-HOPG [39]. In the latter case, the reported measurements correspond to a different collision geometry in forward scattering configuration, even though the calculated neutral fractions (∼20%) presented here are in reasonable agreement with the reported experimental data (between 20% and 30%). Experimentally exploring charge transfer in collisions of Li^+ projectiles colliding with C atoms in backscattering conditions could be rather cumbersome due to the low exit projectile velocities (for typical LEIS incoming energies) caused by the similar atomic mass of the colliding atoms.

IV. CONCLUSIONS

Partial and final projectile charge states of Li projectiles scattered by a graphene surface with K adatoms deposited on it were theoretically determined for different projectile exit velocities in the low-energy range (1–11 keV exit energy). The potassium impurities are assumed to be adsorbed in the very low deposition limit where the interaction between K adatoms can be neglected. We employed a quantum mechanical formalism based on the Anderson Hamiltonian to calculate the scattered ion fractions in head-on projectile-surface collisions, where electronic correlation between the three possible projectile charge channels is included.

Final neutral and negative ion fractions obtained strongly depend on the scattering site, i.e., if the incoming projectile directly collides with the impurity or with the surrounding carbon atoms. For binary collisions with the impurity and the first two nearest carbon atoms, a strong dependence with the projectile outgoing velocity is observed. For these cases, the neutral fraction ranges from almost null for low exit projectile velocities and reaches up to around 50% for larger velocities. For these scattering centers, an important formation of negative ions is observed, averaging around 20% for the whole range of exit velocities explored. When Li^+ projectiles collide with carbon atoms located far from the adsorption site (third nearest neighbors and beyond), around 20% of the scattered projectiles are neutral and this value practically does not depend on the exit projectile energy. The rest (∼80%) of the scattered projectiles mostly remain positive since the formation of negative ions is practically null for the explored energy range.

The analysis of the projectile charge state during its collision trajectory reveals similar features for collisions of Li projectiles with the impurity as well as with the its first nearest C atom neighbor, C_1. Some of these similarities, evidenced in the neutral fraction dependence with the projectile-scatter atom distance, are shifted around the adsorption distance (4.9 a.u.), indicating that they are a direct consequence of the K adatom presence. The differences in the magnitude of neutral fractions obtained can be mainly attributed to both a quite different ionization energy level dependence with the projectile-surface distance and rather different interaction times in the incoming trajectory due to the strong differences in the kinematic loss factor of both collisions.

The assessment of ionization and affinity energy levels with their corresponding hybridization widths allows us to conclude that the strong dependence of the final neutral and negative ion fractions with the exit projectile energy is a direct consequence of the localized features of the K adatom DOS, manifested as peaked interaction widths in the energy levels of the projectile during its collision trajectory. Alternatively, the overall magnitude of the final ion fractions obtained is mainly linked to the position of the ionization and affinity levels relative to the surface Fermi level.

Charge exchange between Li projectiles with carbon atoms located in the surroundings of the K adatom is able to sense the presence of the adsorbate for K-C distances up to around 12.7 a.u. (6.7 Å). For larger K-C distances, no differences are found with final ion fractions calculated for Li projectiles colliding with carbon atoms of a pristine graphene surface. The hybridization widths of the projectile energy levels, however, reveal a non-negligible Li-K interaction for distances up to around 15 a.u., indicating that the Li-K interaction for larger distances is not sufficient to appreciably alter the projectile final charge state for the collision geometry and projectile energy range analyzed.

A direct comparison of the obtained results with those found in collisions of H^+ projectiles with the same surface and under identical collisional geometry allows us to draw conclusions on the relevance of the projectile in the charge exchange with the studied surface. Similar overall values for neutral and negative ion fractions were obtained for both projectiles colliding with the adsorbed K atom, but a stronger (more oscillatory) dependence with the exit velocity is obtained for H^+ projectiles as a consequence of ionization and affinity levels interacting with a larger number of localized states of the K adatom. Strong differences for both projectiles are obtained when contrasting the neutral fractions for collisions with a C atom located far away from the adsorbate, as a consequence of a much deeper H^+ ionization energy level resonating with the graphene valence band. In contrast to the strong dependence of charge fractions with the exit projectile velocity in collisions with the K adatom, a soft dependence is observed for both projectiles colliding with C atoms of a clean graphene surface mainly due to the extended nature of the graphene DOS.

Finally, the theoretical results presented here are intended to serve as a predictive and analytical tool for charge exchange analysis in more complex surfaces. However, we understand that validating the calculations performed here with proper experiments is absolutely necessary. Several experimental difficulties, such as sample preparation and the LEIS related issues mentioned above, should be primarily overcome in order to achieve this goal.

ACKNOWLEDGMENT

This work was supported by CONICET through Grant No. PIP-2021-101517, ANPCyT through Grant No. PICT-2019-03943, and U.N.L. through CAI+D grants.

---

[1] J. Los and J. J. C. Geerlings, Charge exchange in atom-surface collisions, Phys. Rep. **190**, 133 (1990).

[2] A. G. Borisov, D. Teillet-Billy, J. P. Gauyacq, H. Winter, and G. Dierkes, Resonant charge transfer in grazing scattering of alkali-metal ions from an Al(111) surface, Phys. Rev. B **54**, 17166 (1996).

[3] A. G. Borisov, A. K. Kazansky, and J. P. Gauyacq, Resonant charge transfer in ion-metal surface collisions: Effect of a

projected band gap in the H^--Cu(111) system, Phys. Rev. B **59**, 10935 (1999).

[4] B. Bahrim, B. Makarenko, and J. W. Rabalais, Mechanism of negative ion formation in low velocity collisions at surfaces, Surf. Sci. **542**, 161 (2003).

[5] E. A. García, C. G. Pascual, P. G. Bolcatto, M. C. G. Passeggi, and E. C. Goldberg, Ion fractions in the scattering of hydrogen on different reconstructed silicon surfaces, Surf. Sci. **600**, 2195 (2006).

[6] F. Bonetto, M. A. Romero, E. A. García, R. Vidal, J. Ferrón, and E. C. Goldberg, Relevant effects of localized atomic interactions and surface density of states on charge transfer in ion-surface collisions, Europhys. Lett. **80**, 53002 (2007).

[7] D. Primetzhofer, M. Spitz, E. Taglauer, and P. Bauer, Resonant charge transfer in low-energy ion scattering: Information depth in the reionization regime, Surf. Sci. **605**, 1913 (2011).

[8] R. A. Vidal, F. Bonetto, J. Ferrón, M. A. Romero, E. A. García, and E. C. Goldberg, Electron capture and loss in the scattering of H^+ from HOPG graphite, Surf. Sci. **605**, 18 (2011).

[9] A. Iglesias-García, C. González, and E. C. Goldberg, Theoretical study of the charge transfer and electron emission in the scattering of He^+ by an AlF_3 surface, Phys. Rev. B **96**, 075428 (2017).

[10] I. K. Gainullin, Resonant charge transfer during ion scattering on metallic surfaces, Phys.-Usp. **63**, 888 (2020).

[11] M. Maazouz, A. G. Borisov, V. A. Esaulov, J. P. Gauyacq, L. Guillemot, S. Lacombe, and D. Teillet-Billy, Effect of metal band characteristics on resonant electron capture: H^- formation in the scattering of hydrogen ions on Mg, Al, and Ag surfaces, Phys. Rev. B **55**, 13869 (1997)

[12] M. Maazouz, L. Guillemot, T. Schlatholter, S. Ustaze, and V. A. Esaulov, Electron capture and loss in the scattering of oxygen atoms and ions on Mg, Al and Ag surfaces, Nucl. Instrum. Methods Phys. Res., Sect. B **125**, 283 (1997).

[13] Y. Yang and J. A. Yarmoff, Charge Exchange in Li Scattering from Si Surfaces, Phys. Rev. Lett. **89**, 196102 (2002).

[14] A. R. Canário, T. Kravchuk, and V. A. Esaulov, Bandgaps, surface states and the anomalous neutralization of Li^+ on (111) surfaces of noble metals, New J. Phys. **8**, 227 (2006).

[15] N. B. Luna, F. J. Bonetto, R. A. Vidal, E. C. Goldberg, and J. Ferrón, Low energy ion scattering in He/HOPG system, J. Mol. Catal. A: Chem. **281**, 237 (2008).

[16] X. He and J. A. Yarmoff, Correlated Electron Effects in Low Energy Sr^+ Ion Scattering, Phys. Rev. Lett. **105**, 176806 (2010).

[17] C. Meyer, F. Bonetto, R. Vidal, E. A. García, C. Gonzalez, J. Ferrón, and E. C. Goldberg, Understanding the high neutralization yields in collisions of keV Li^+ ions with copper surfaces, Phys. Rev. A **86**, 032901 (2012).

[18] A. B. Arjad and J. A. Yarmoff, Temperature dependence of the neutralization of low energy K^+ ions scattered from Au nanoclusters on SiO_2, Nucl. Instrum. Methods Phys. Res., Sect. B **317**, 13 (2013).

[19] F. J. Bonetto, E. A. García, C. González, and E. C. Goldberg, Image Potential State Influence on Charge Exchange in Li^+–Metal Surface Collisions, J. Phys. Chem. C **118**, 8359 (2014).

[20] A. Iglesias-García, F. Bonetto, R. Vidal, J. Ferrón, and E. C. Goldberg, Ion neutralization and high-energy electron emission in He^+ scattering by a highly oriented pyrolitic graphite surface, Phys. Rev. A **89**, 042702 (2014).

[21] F. Bonetto, C. Gonzalez, and E. C. Goldberg, Signals of strong electronic correlation in ion scattering processes, Phys. Rev. B **93**, 195439 (2016).

[22] M. S. Tacca, F. Bonetto, and E. C. Goldberg, Electronic correlation effects on the neutralization of Ga^+ scattered by a gold surface, Phys. Rev. B **96**, 075424 (2017).

[23] V. Q. Riascos, M. Tacca, R. Vidal, C. Gonzalez, E. C. Goldberg, and F. Bonetto, Band Structure Effects on the Charge Exchange Processes in H^+ Colliding with a Cu(111) Surface, J. Phys. Chem. C **122**, 28192 (2018).

[24] M. Tacca, V. Quintero Riascos, R. Vidal, C. Gonzalez, F. Bonetto, and E. C. Goldberg, Charge Transfer in Low-Energy Collisions of Protons with a Thick C60 Film, J. Phys. Chem. C **124**, 3632 (2020).

[25] V. Quintero Riascos, M. Tacca, R. Vidal, C. Gonzalez, E. C. Goldberg, and F. Bonetto, Electron capture and loss in the scattering of low-energy protons with a C60 monolayer deposited on Cu(111), Phys. Rev. A **103**, 062805 (2021).

[26] F. Bonetto, E. A. García, R. Vidal, J. Ferrón, and E. C. Goldberg, Experimental and theoretical study of charge transfer in hydrogen ion scattering from a graphite surface, Appl. Surf. Sci. **254**, 62 (2007).

[27] H. D. Hagstrum, Theory of Auger ejection of electrons from metals by ions, Phys. Rev. **96**, 336 (1954).

[28] R. Souda, M. Aono, C. Oshima, S. Otani, and Y. Ishizawa, Mechanism of electron exchange between low energy He^+ and solid surfaces, Surf. Sci. Lett. **150**, L59 (1985).

[29] S. N. Mikhailov, L. C. A. van den Oetelaar, and H. H. Brongersma, Strong matrix effect in low-energy He^+ ion scattering from carbon, Nucl. Instrum. Methods Phys. Res., Sect. B **93**, 210 (1994).

[30] T. Li and R. J. MacDonald, Inelastic energy loss and charge exchange in low-energy heavy ions scattered from Cu and Cu-alloy surfaces, Phys Rev B **51**, 17876 (1995).

[31] R. Souda, K. Yamamoto, W. Hayami, B. Tilley, T. Aizawa, and Y. Ishizawa, Neutralization and negative-ion formation by impact of low-energy H^+ on ionic compound surfaces, Surf. Sci. **324**, L349 (1995).

[32] M. Draxler, R. Gruber, H. H. Brongersma, and P. Bauer, Velocity Scaling of Ion Neutralization in Low Energy Ion Scattering, Phys. Rev. Lett. **89**, 263201 (2002).

[33] S. Průša, P. Procházka, P. Bábor, T. Šikola, R. ter Veen, M. Fartmann, T. Grehl, P. Brüner, D. Roth, P. Bauer, and H. H. Brongersma, Highly sensitive detection of surface and intercalated impurities in graphene by LEIS, Langmuir **31**, 9628 (2015).

[34] B. Bahrim, S. Yu, B. Makarenko, and J. W. Rabalais, Electron dynamics in H^-/Na/Cu(111) collisions, Surf. Sci. **603**, 703 (2009).

[35] S. Yu, B. Bahrim, B. Makarenko, and W J., Rabalais, H^- survival probability during collisions with Na/Cu(111), Surf. Sci. **636**, 13 (2015).

[36] B. Bahrim, J. Stafford, and B. Makarenko, Charge transfer during H/H^- collisions with Cu(100) and Cu(111) surfaces, Surf. Interface Anal. **50**, 212 (2018).

[37] B. Bahrim, H^- ion fractions scattered from Ag(111) and polycrystalline Ag, Surf. Sci. **706**, 121781 (2021).

[38] B. Bahrim, Local effects during ion scattering on adsorbate-covered surfaces, Surf. Sci. **726**, 122176 (2022).

[39] F. Bonetto, M. A. Romero, E. A. García, R. A. Vidal, J. Ferrón, and E. C. Goldberg, Large neutral fractions in collisions of Li^+ with a highly oriented pyrolytic graphite surface: Resonant and Auger mechanisms, Phys. Rev. B **78**, 075422 (2008).

[40] E. A. García, M. A. Romero, C. González, and E. C. Goldberg, Neutralization of Li^+ ions scattered by the Cu (100) and (111) surfaces: A localized picture of the atom-surface interaction, Surf. Sci. **603**, 597 (2009).

[41] A. Iglesias-García, A. G. Evelina, and E. C. Goldberg, Localized description of surface energy gap effects in the resonant charge exchange between atoms and surfaces, J. Phys.: Condens. Matter **23**, 045003 (2011).

[42] A. Iglesias-García, E. A. García, and E. C. Goldberg, Role of He excited configurations in the neutralization of He^+ ions colliding with a HOPG surface, Phys. Rev. B **87**, 075434 (2013).

[43] F. J. Bonetto, M. A. Romero, A. Iglesias-García, R. A. Vidal, and E. C. Goldberg, Time–energy uncertainty and electronic correlation in H^+–graphite collisions, J. Phys. Chem. C **119**, 3124 (2015).

[44] A. Iglesias-García, M. A. Romero, E. A. García, and E. C. Goldberg, Collision of protons with carbon atoms of a graphene surface in the presence of adsorbed potassium, Phys. Rev. B **102**, 115406 (2020).

[45] H. H. Brongersma, M. Draxler, M. de Ridder, and P. Bauer, Surface composition analysis by low-energy ion scattering, Surf. Sci. Rep. **62**, 63 (2007).

[46] H. R. J. ter Veen, T. Kim, I. E. Wachs, and H. H. Brongersma, Applications of high sensitivity-low energy ion scattering (HS-LEIS) in heterogeneous catalysis, Catal. Today **140**, 197 (2009).

[47] T. A. Flaim and P. D. Ownby, Adsorbate-induced work function changes, Surf. Sci. **32**, 519 (1972).

[48] V. De Renzi, R. Rousseau, D. Marchetto, R. Biagi, S. Scandolo, and U. del Pennino, Metal Work-Function Changes Induced by Organic Adsorbates: A Combined Experimental and Theoretical Study, Phys. Rev. Lett. **95**, 046804 (2005).

[49] J. P. Gauyacq and A. G. Borisov, Charge transfer in atom-surface collisions: Effect of the presence of adsorbates on the surface, J. Phys.: Condens. Matter **10**, 6585 (1998).

[50] A. G. Borisov, J. P. Gauyacq, E. V. Chulkov, V. M. Silkin, and P. M. Echenique, Lifetime of excited electronic states at surfaces: Comparison between the alkali/Cu(111) systems, Phys. Rev. B **65**, 235434 (2002).

[51] J. A. Yarmoff, Y. Yang, and Z. Sroubek, Imaging the Internal Electronic Structure of a Surface Adsorbate with Low Energy Ions, Phys. Rev. Lett. **91**, 086104 (2003).

[52] Y. Yang, Z. Sroubek, and J. A. Yarmoff, Internal electronic structure of adatoms on Fe(110) and Fe(100) surfaces: A low-energy Li^+ scattering study, Phys. Rev. B **69**, 045420 (2004).

[53] S. Yu, B. Bahrim, B. Makarenko, and J. W. Rabalais, Local effect of Na adsorption on Cu(111), Surf. Sci. **606**, 1700 (2012).

[54] L. Gao, Y. Zhu, Y. Shi, P. Liu, Y. Xiao, F. Ren, L. Chen, Y. Guo, and X. Chen, Role of projectile energy and surface work function on charge transfer of negative ions grazing scattering on dissociated $\mathrm{H_2O}$-covered Cu(110), Appl. Surf. Sci. **428**, 1082 (2018).

[55] E. A. García, A. Iglesias-García, S. C. Gómez Carrillo, and M. A. Romero, *S*-type single alkali-adatom on graphene, Appl. Surf. Sci. **452**, 507 (2018).

[56] M. A. Romero, A. Iglesias-García, E. A. García, and E. C. Goldberg, Hydrogen ion scattering from a potassium impurity adsorbed on graphene, Phys. Rev. B **100**, 085432 (2019).

[57] M. A. Romero, A. Iglesias-García, and E. A. García, Hydrogen ion scattering from alkali/graphene surface: Alkali core states effects, Surf. Sci. **721**, 122070 (2022).

[58] G. F. Liu, Z. Sroubek, P. Karmakar, and J. A. Yarmoff, Li ion scattering from Au nanoclusters on $\mathrm{TiO_2}$(110), J. Chem. Phys. **125**, 054715 (2006).

[59] R. D. Gann, Z. Sroubek, and J. A. Yarmoff, Dopant enhanced neutralization of low-energy Li^+ scattered from Si(111), Phys. Rev. B **85**, 165307 (2012).

[60] J. J. C. Geerlings, L. F. T. Kwakman, and J. Los, Local work function effects in the neutralization of alkali ions scattered from cesiated surfaces, Surf. Sci. **184**, 305 (1987).

[61] P. W. Anderson, Localized magnetic states in metals, Phys. Rev. **124**, 41 (1961).

[62] A. C. Hewson, *The Kondo Problem to Heavy Fermions*, Cambridge Studies in Magnetism (Cambridge University Press, Cambridge, 1993).

[63] M. A. Romero, F. Flores, and E. C. Goldberg, Effective treatment of charge and spin fluctuations in dynamical and static atom-surface interactions, Phys. Rev. B **80**, 235427 (2009).

[64] P. G. Bolcatto, E. C. Goldberg, and M. C. G. Passeggi, Test of a bond-pair superposition model describing the interaction between atoms: Application to the hydrides of the first-row elements, Phys. Rev. A **50**, 4643 (1994).

[65] P. G. Bolcatto, E. C. Goldberg, and M. C. G. Passeggi, Interaction between atoms and surfaces: A bond-pair description based on an extended Anderson model, Phys. Rev. B **58**, 5007 (1998).

[66] M. A. Romero and E. C. Goldberg, Local density of states of atoms interacting with finite-bandwidth surfaces: Spin-statistics effects, Phys. Rev. B **74**, 195419 (2006).

[67] P. Jelínek, H. Wang, J. P. Lewis, O. F. Sankey, and J. Ortega, Multicenter approach to the exchange-correlation interactions in *ab initio* tight-binding methods, Phys. Rev. B **71**, 235101 (2005).

[68] J. P. Lewis *et al.*, Advances and applications in the FIREBALL *ab initio* tight-binding molecular-dynamics formalism, Phys. Status Solidi **248**, 1989 (2011).

[69] L. V. Keldysh, Diagram technique for nonequilibrium processes, Sov. Phys. JETP **20**, 1018 (1965).

[70] Z. H. Zhu and G. Q. Lu, Comparative study of Li, Na, and K adsorptions on graphite by using *ab initio* method, Langmuir **20**, 10751 (2004).

[71] K. Rytkönen, J. Akola, and M. Manninen, Density functional study of alkali-metal atoms and monolayers on graphite (0001), Phys. Rev. B **75**, 075401 (2007).

[72] N. Dimakis, D. Valdez, F. A. Flor, A. Salgado, K. Adjibi, S. Vargas, and J. Saenz, Density functional theory calculations on alkali and the alkaline Ca atoms adsorbed on graphene monolayers, Appl. Surf. Sci. **413**, 197 (2017).

[73] S. Huzinaga, J. Andzelm, M. Klobukowsky, E. Radzio-Andzelm, Y. Sakai, and H. Tatewaki, *Gaussian Basis Sets for Molecular Calculations*, Vol. 16 (Elsevier Science Publishers B. V., Amsterdam, 1984).

[74] K. Oura, V. G. Lifshits, A. A. Saranin, A. V. Zotov, and M. Katayama, *Surface Science: An Introduction* (Springer-Verlag, New York, 2003).

[75] B. Bahrim, B. Makarenko, and J. W. Rabalais, Band gap effect on H^- ion survival near Cu surfaces, Surf. Sci. **594**, 62 (2005).

[76] C. V. Cushman, P. Bruner, J. Zakel, G. H. Major, B. M. Lunt, N. J. Smith, T. Grehl, and M. R. Linford, Low energy ion scattering (LEIS). A practical introduction to its theory, instrumentation, and applications, Anal. Methods **8**, 3419 (2016).

[77] K. A. H. German, C. B. Weare, P. R. Varekamp, J. N. Andersen, and J. A. Yarmoff, Site-Specific Neutralization of Low Energy Li^+ Scattered from Na/Al(100), Phys. Rev. Lett. **70**, 3510 (1993).

[78] Q. B. Lu, R. Souda, D. J. O'Connor, and B. V. King, Electronic-Structure Modification and the Adsorption Site of Oxygen on Alkali (Cs) Covered Surfaces Studied by Normal Exit Li^- Ion Spectroscopy, Phys. Rev. Lett. **77**, 3236 (1996).